COMMUNICATIONS PHYSICS

ARTICLE

https://doi.org/10.1038/s42005-020-00463-6 OPEN

Topological Josephson heat engine

Benedikt Scharf [1✉], Alessandro Braggio [2], Elia Strambini [2], Francesco Giazotto [2] & Ewelina M. Hankiewicz[1]

Topological superconductors represent a fruitful playing ground for fundamental research as well as for potential applications in fault-tolerant quantum computing. Especially Josephson junctions based on topological superconductors remain intensely studied, both theoretically and experimentally. The characteristic property of these junctions is their 4π-periodic ground-state fermion parity in the superconducting phase difference. Using such topological Josephson junctions, we introduce the concept of a topological Josephson heat engine. We discuss how this engine can be implemented as a Josephson–Stirling cycle in topological superconductors, thereby illustrating the potential of the intriguing and fruitful marriage between topology and coherent thermodynamics. It is shown that the Josephson–Stirling cycle constitutes a highly versatile thermodynamic machine with different modes of operation controlled by the cycle temperatures. Finally, the thermodynamic cycle reflects the hallmark 4π-periodicity of topological Josephson junctions and could therefore be envisioned as a complementary approach to test topological superconductivity.

[1] Institute for Theoretical Physics and Astrophysics and Würzburg-Dresden Cluster of Excellence ct.qmat, University of Würzburg, Am Hubland, 97074 Würzburg, Germany. [2] NEST, Istituto Nanoscienze-CNR and Scuola Normale Superiore, 56127 Pisa, Italy. ✉email: benedikt.scharf@ur.de

The promise of fault-tolerant quantum computing has made topological superconductors the focus of intense research during the past decade[1,2]. In this context, topological Josephson junctions based on nanowires[3,4] or on topological insulators[5–11] provide an alternative route for probing topological superconductivity. Their topological nature is reflected in a ground-state fermion parity that is 4π-periodic in the superconducting phase difference ϕ. Finding unambiguous experimental evidence for this 4π-periodicity still proves a difficult task, however[12–16], and it is therefore desirable to have several different and complementary approaches. Here we propose a topological Josephson heat engine implemented by a Josephson–Stirling cycle and discuss its thermodynamic[17–23] properties. Using a Josephson junction based on a quantum spin Hall (QSH) insulator as an example, we show how topological Josephson junctions represent versatile thermodynamic machines with various operating modes. Moreover, the thermodynamic cycle properties reflect the 4π-periodicity of the topological ground state, distinguishing between parity-conserving and non-parity-conserving engines. Interestingly, we find that parity conservation generally boosts both the efficiency and power of the topological heat engine with respect to its non-topological counterpart. Our results are applicable not only to QSH-based junctions but also to any topological Josephson junction and establish topological Josephson heat engines as a novel testbed for the 4π-periodicity of the ground-state fermion parity by its entropic signature.

Results and discussion

Basic ideas. In our proposed set-up (Fig. 1a), an external magnetic flux controls the superconducting phase bias ϕ across the junction. The temperature T of the QSH system is assumed to be externally modulated compared to the bath temperature T_b. For example, this could be done with radiative heating of the system[24–26] or by having the superconductors acting as reservoirs whose temperature is controlled via resistors or superconductor/insulator/superconductor tunnel junctions[17].

A Josephson–Stirling cycle[23] is composed by a sequence of (i) an isothermal phase change of $\phi = 0 \to \phi_f$ at an externally set temperature $T = T_e$, followed by (ii) an isophasic temperature change $T = T_e \to T_b$ at constant $\phi = \phi_f$, (iii) an isothermal phase change of $\phi = \phi_f \to 0$ at $T = T_b$, and (iv) an isophasic temperature change $T = T_b \to T_e$ at $\phi = 0$ to complete the cycle (Fig. 1b). If the reference phase ϕ_f is chosen as (an integer multiple of) $\phi_f = 2\pi$, the work released by the engine crucially differs between a set-up without fermion-parity constraints and a set-up with constant fermion parity. In the former case, the free energy and other thermodynamic quantities are 2π-periodic. This requires that no work or heat is generated or absorbed during each of the isothermal phase changes $\phi = 0 \to 2\pi$ and $\phi = 2\pi \to 0$. If we assume, on the other hand, that the fermion parity can be kept constant throughout all processes, the thermodynamic quantities are 4π-periodic. Work and heat are then exchanged with the reservoirs during the isothermal phase changes $\phi = 0 \to 2\pi$ and $\phi = 2\pi \to 0$. Hence, for $\phi_f = 2\pi$ a topological heat engine releases work only when parity can be conserved (Fig. 1c, d).

Model and thermodynamic properties. While the concepts outlined above are expected for any topological Josephson junction, we will discuss them explicitly for the example of a short, topological Josephson junction based on a QSH insulator. Here the pairing in the superconducting (S) regions is induced from nearby *s*-wave superconductors (see Fig. 1a, also for the coordinate system). Assuming two independent edges of the QSH system, the corresponding Bogoliubov-de Gennes Hamiltonian for the QSH edge states then reads

$$\hat{H}_{s,\sigma} = \left(s\sigma v_F \hat{p}_x - \mu_S\right)\tau_z + V_0 L_N \delta(x)\tau_z + \Delta\left[\tau_x \cos\Phi(x) - \tau_y \sin\Phi(x)\right], \quad (1)$$

where $s = \uparrow/\downarrow \equiv \pm 1$ describes the natural (out-of-plane) spin projection, $\sigma = t/b \equiv \pm 1$ the top and bottom edges, and τ_j (with

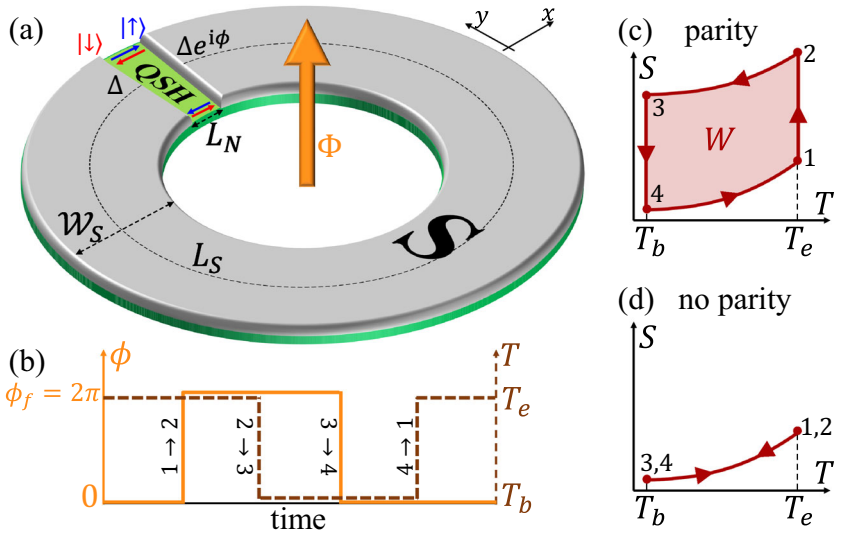

Fig. 1 Concept of a topological Josephson heat engine. a Scheme: a quantum spin Hall (QSH) insulator is partially covered by an *s*-wave superconductor (*S*), which proximity-induces pairing into the QSH edge states $|\uparrow\rangle$ and $|\downarrow\rangle$, thus defining (proximitized) superconducting regions. A magnetic flux Φ induces a superconducting phase difference ϕ across the normal QSH weak link. The proximitized QSH system is at temperature T. **b** Timeline defining the four sequences of ϕ and T to implement the Josephson–Stirling thermodynamic cycle: $1 \equiv (\phi = 0, T_e)$, $2 \equiv (\phi = \phi_f, T_e)$, $3 \equiv (\phi = \phi_f, T_b)$ and $4 \equiv (\phi = 0, T_b)$. **c**, **d** Josephson–Stirling cycle in the (T, S) plane for $\phi_f = 2\pi$ with and without parity conservation, respectively. Here S is the total entropy of the system. The area enclosed by the cycle in the (T, S) plane corresponds to the total heat Q absorbed, which is equivalent to the total work W done during the cycle. In this set-up, $W \neq 0$ only if parity is conserved due to the trivial 2π-periodicity of the non-topological engine.

$j = x, y, z$) denote Pauli matrices of the particle-hole degrees of freedom (see Supplementary Notes I).

We study a short junction with a normal QSH region of width L_N, approximated by a δ-like profile. The proximity-induced pairing amplitude is Δ and we use the phase convention $\Phi(x) = \Theta(x)\phi$ to describe the superconducting phase difference ϕ between the two S regions. Furthermore, $\hat{p}_x$ denotes the momentum operator, and V_0 is the potential difference between the normal QSH and proximitized S regions. We employ a scattering approach to determine the Andreev bound states and the continuum spectrum of Eq. (1), from which we obtain the free energy—up to some additive ϕ-independent contributions—as

$$F_0(\phi, T) = -2k_B T \ln\left[2\cosh\left(\frac{\Delta\cos\frac{\phi}{2}}{2k_B T}\right)\right] \quad (2)$$

with the Boltzmann constant k_B and the temperature T of the QSH states (see Supplementary Notes II and III). Here Eq. (2) arises solely from the Andreev bound state energies and the prefactor 2 takes into account contributions from the top and bottom edges.

Equation (2) describes a situation where the states of the system have equilibrium occupations without any external constraints. If fermion-parity conservation is enforced, the free energy acquires an additional term and becomes

$$F_p(\phi, T) = -2k_B T \ln\left[\cosh\left(\frac{\Delta\cos\frac{\phi}{2}}{2k_B T}\right) + pe^{J_S(T)}\sinh\left(\frac{\Delta\cos\frac{\phi}{2}}{2k_B T}\right)\right], \quad (3)$$

where we use the convention that $p = \pm 1$ corresponds to even and odd ground-state parity, respectively. In Eq. (3), we again omit additive ϕ-independent contributions to F_p, which are also parity independent. The contribution

$$J_S(T) = -\frac{2}{\pi k_B T E_S}\int_\Delta^\infty d\epsilon\ \frac{\sqrt{\epsilon^2 - \Delta^2}}{\sinh(\epsilon/k_B T)} \quad (4)$$

originates from the superconducting electrodes, where the energy scale $E_S = \hbar v_F/L_S$ is related to the total length L_S of the superconducting QSH edge[7]. Following refs. [7,27], we have assumed rigid boundary conditions in writing down Eqs. (2) and (3) and do therefore not take into account the inverse proximity effect since $L_S \gg L_N$[21].

The total free energy F of the QSH junction, given by Eq. (2) or (3), allows us to calculate the total Josephson current via[27]

$$I(\phi, T) = \frac{2e}{\hbar}\frac{\partial F(\phi, T)}{\partial\phi}, \quad (5)$$

where e is the elementary charge, and the entropy via

$$S(\phi, T) = -\frac{\partial F(\phi, T)}{\partial T}. \quad (6)$$

From S, one can subsequently obtain the heat capacity of the junction

$$C(\phi, T) = T\frac{\partial S(\phi, T)}{\partial T}. \quad (7)$$

Importantly, Eq. (2) is 2π-periodic in ϕ, while Eq. (3) is 4π-periodic. Consequently, the quantities derived from Eq. (2) or (3) inherit the respective periodicities. This is illustrated by Fig. 2a, b, which shows F and S for junctions without and with parity constraints. For simplicity, we assume a temperature-independent proximity gap, $\Delta(T) \approx \Delta(T = 0)$ and $\partial\Delta/\partial T \approx 0$, during our calculations, which is reasonably valid for the set-up considered here (see Supplementary Notes III).

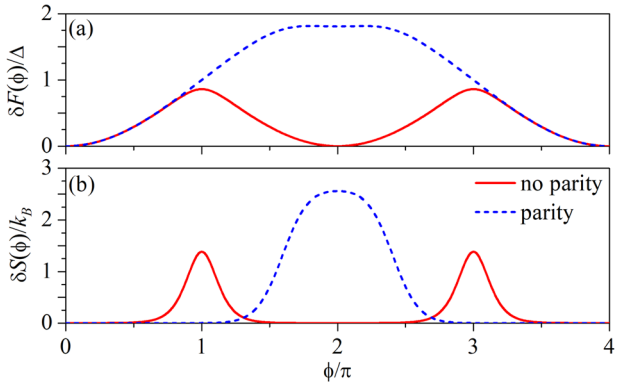

Fig. 2 Phase-dependent thermodynamic quantities. a Phase-dependent variation of the total free energy $\delta F(\phi) = F(\phi) - F(0)$ and **b** entropy $\delta S(\phi) = S(\phi) - S(0)$ of the system for $k_B T = 0.1\Delta$ and $E_S = 0.165\Delta$ without [$F = F_0$ given by Eq. (2)] and with parity constraints [$F = F_p$ given by Eq. (3)]. If parity constraints are enforced, we choose the branch $p = 1$. In contrast to the current I, the exact values of F and S (as well as C) at a given ϕ also require knowledge of the ϕ-independent contributions omitted in Eqs. (2) and (3). To overcome this difficulty, we measure F and S with respect to their values at $\phi = 0$, thereby canceling the offset due to the ϕ-independent contributions.

Thermodynamic processes. For the Josephson–Stirling cycle, we need to describe different thermodynamic processes. We study quasi-static processes, during which the system passes through quasi-equilibrium states. Then the work done and heat released during a process $i \to f$ are $W_{i\to f} = -\hbar/(2e)\int d\phi\, I(\phi, T)$ and $Q_{i\to f} = \int dS\, T$, respectively. The sign convention is such that $W_{i\to f}$ is positive when the system releases work to the environment, while $Q_{i\to f}$ is positive when the system absorbs heat from the environment.

For an isothermal process where ϕ is changed from $\phi_i \to \phi_f$ at constant T, $W_{i\to f} = -[F(\phi_f, T) - F(\phi_i, T)]$ and $Q_{i\to f} = T[S(\phi_f, T) - S(\phi_i, T)]$ can be directly obtained from Eqs. (2) and (3) and their temperature derivatives. During an isophasic process, T is changed from $T_i \to T_f$ at constant ϕ. In this case, $W_{i\to f} = 0$, while

$$Q_{i\to f} = \int_{T_i}^{T_f} dT\ [C_0(T) + \delta C(\phi, T)] \quad (8)$$

can be calculated from the total heat capacity. The ϕ-dependent contribution $\delta C(\phi, T) = C(\phi, T) - C_0(T)$ can be directly calculated from Eq. (2) or (3) and its derivatives and is measured with respect to $\phi = 0$. In principle, we also need to account for the ϕ-independent contribution $C_0(T)$ arising from the terms omitted in Eqs. (2) and (3). For additional details, we refer to Supplementary Notes IV and V, where $C_0(T)$ is calculated using the Bardeen–Cooper–Schrieffer density of states.

Josephson–Stirling cycle. We are now in a position to explicitly compute the total work and heat produced during each of the processes of the Josephson–Stirling cycle introduced above (Fig. 1b). As mentioned above, $W_{1\to 2}$ and $W_{3\to 4}$ correspond to integrals over the current–phase relation but can also be computed directly from F. The total work $W = W_{1\to 2} + W_{3\to 4}$ of each cycle thus coincides with the difference between the integrated areas over the current–phase relation (Fig. 3a, b). The heat exchanged with the hot ($T = T_e$) and cold reservoirs ($T = T_b$) is $Q_e = Q_{1\to 2} + Q_{4\to 1}$ and $Q_b = Q_{2\to 3} + Q_{3\to 4}$, respectively. Conservation of energy dictates $W = Q$, where $Q = Q_e + Q_b$ is the total heat exchange during the cycle. Note that, in our set-up, there are no separate hot and cold reservoirs, but the environment acts successively as hot and cold reservoir.

In Fig. 3c, we show W as a function of the reference phase ϕ_f and compare the case without and with parity constraints. Without parity conservation, W is maximal for $\phi_f = \pi$, whereas $W = 0$ for $\phi_f = 2\pi$. The latter is a consequence of the 2π-periodicity of $F_0(\phi,\ T) = F_0(\phi + 2\pi,\ T)$, causing $W_{1\to2} = -[F_0(\phi_f,\ T_e) - F_0(0,\ T_e)]$ and $W_{3\to4} = -F_0(0,\ T_b) - F_0(\phi_f,\ T_b)]$ to each vanish for $\phi_f = 2\pi$. If fermion parity is kept constant, on the other hand, $F_p(\phi,\ T) = F_p(\phi + 4\pi,\ T)$ and W is maximal for $\phi_f = 2\pi$. A topological heat engine with $\phi_f = 2\pi$ thus releases work only if parity is conserved and can thus serve as a test for the 4π-periodicity of the ground-state fermion parity.

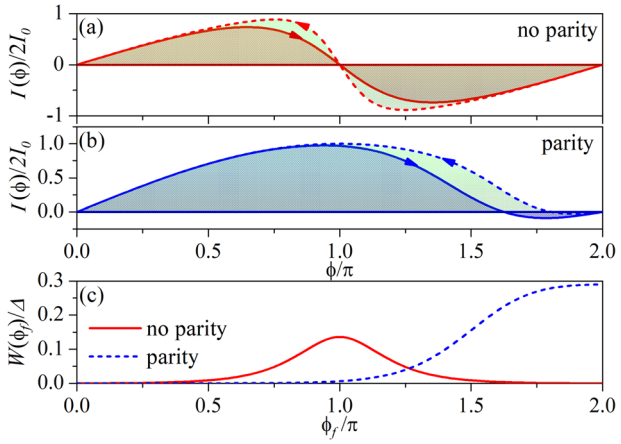

Fig. 3 Current-phase relation and work. a, **b** Isothermal current-phase relation at $k_BT = 0.1\Delta$ (dashed lines) and $k_BT = 0.2\Delta$ (solid lines) **a** without and **b** with parity constraints. Here the shaded areas between each curve and the ϕ axis correspond to the work performed during an isothermal change $\phi = 0 \to 2\pi$. The areas above and below the ϕ axis compensate each other in **a** for an isothermal change $\phi = 0 \to 2\pi$ and no work is released. In **a**, **b**, the arrows indicate the direction of the changes in ϕ for a Josephson–Stirling engine with $k_BT_e = 0.2\Delta$, $k_BT_b = 0.1\Delta$, and $\phi_f = 2\pi$. The total work W performed by these engines is represented by the shaded green areas between the dashed and solid curves. **c** Total work W released by a Josephson–Stirling engine with $k_BT_e = 0.2\Delta$ and $k_BT_b = 0.1\Delta$ as a function of the maximal phase change ϕ_f during the cycle. In all panels, $E_S = 0.165\Delta$.

Different operating modes. Until now, we have focused only on an engine. Depending on the relative values of T_e and T_b, the Josephson–Stirling cycle can, however, exhibit also other operating modes. This is illustrated by Fig. 4, which shows W and cycle efficiencies for different combinations of T_e and T_b without (Fig. 4a, b) and with (Fig. 4c, d) parity constraints. Here ϕ_f is chosen to yield the maximal work, that is, $\phi_f = \pi$ without parity constraints (Fig. 4a) and $\phi_f = 2\pi$ if parity is conserved (Fig. 4c).

For $T_e > T_b$, the Josephson–Stirling cycle/machine acts as an engine: The machine absorbs $Q_e > 0$ from the hot reservoir and releases $|Q_b| < Q_e$ to the cold reservoir. Hence, $W > 0$ is done on the environment and the engine efficiency is given by $\eta = W/Q_e$. A comparison of the engine efficiency and maximal power shows that a parity-conserving engine is on average more efficient and more powerful than its non-parity-conserving implementation (Fig. 4b, d). We interpret the stronger power as due to an increased phase space available: to obtain a finite work, the work integral can be integrated over a 0–2π range if parity is preserved, whereas one needs to remain within the 0–π range without parity conservation. Second, the lower efficiency of the non-parity-conserving engine can be understood as due to the competition between mutually exclusive processes with opposite parities. Indeed, Eq. (3) shows that the additional parity-related terms contribute with different signs to F_p, implying opposite contributions to the heat exchange. Consequently, the non-parity-preserving engine can be interpreted as a thermal machine composed of two mutually exclusive engines working in an opposite manner, thereby reducing the total efficiency.

If $T_e < T_b$, the systems with and without parity conservation act as refrigerators with a coefficient of performance $\mathrm{COP} = Q_e/|W|$[23] or as Joule or cold pumps. Controlling T_e vs T_b thus enables

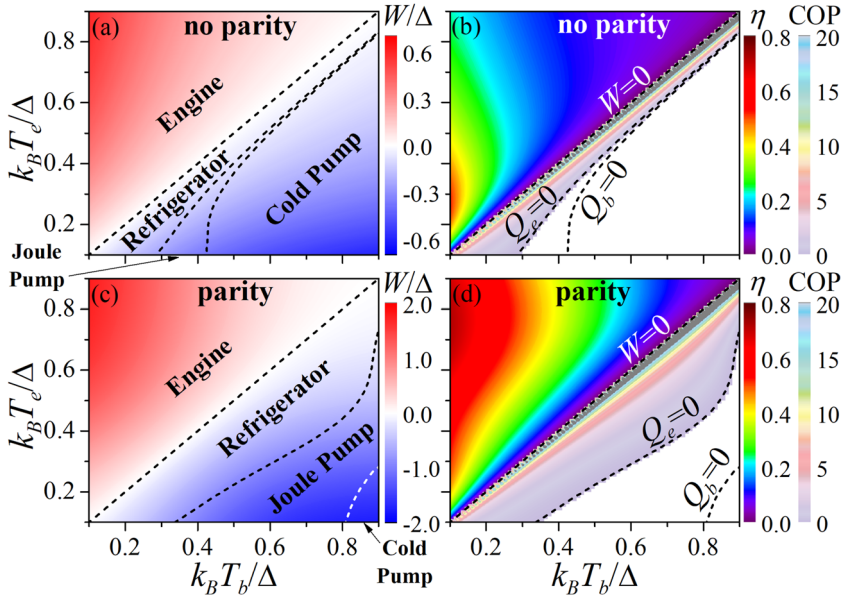

Fig. 4 Josephson–Stirling cycle. Total work W and efficiency η or coefficient of performance (COP) as functions of the reservoir temperatures T_e and T_b **a**, **b** without and **c**, **d** with parity constraints. In both cases, $E_S = 0.165\Delta$. The different operating modes of the cycle are indicated in panels **a**, **c**: for refrigerators, the cycle absorbs heat Q_e from the cooled subsystem with temperature T_e and releases heat $Q_b < 0$ with $|Q_b| > Q_e$ to the heat sink with temperature T_b. If $T_e < T_b$, $Q_e < 0$, and $Q_b < 0$, the machine is a Joule pump that completely converts work into heat released to the reservoirs. On the other hand, if $T_e < T_b$, $Q_e < 0$, and $W < 0$, while $Q_b > 0$, the machine acts as a cold pump transferring heat from the hot ($T = T_b$) to the cold reservoir ($T = T_e$).

multiple operating modes of the Josephson–Stirling cycle. If the cycle is set up as in Fig. 1b, refrigerators as well as Joule and cold pumps require that $T_e < T_b$. While it is possible by superconductor/insulator/superconductor cooling to bring T_e below T_b[17], a more promising way to realize refrigerators, Joule, or cold pumps is to shift the cycle by interchanging the initial and final phases, $\phi = 0$ and $\phi = \phi_f$. Such a set-up implies the same phase diagrams as in Fig. 4 but with T_e and T_b interchanged (see Supplementary Notes VI). Hence the "shifted" Josephson–Stirling cycle can be used to realize operating modes other than engines, making it a highly versatile thermodynamic machine.

Potential routes to experimental realization. Importantly, a topological Josephson heat engine implemented as a Josephson–Stirling cycle can be used to test the hallmark 4π-periodicity of the phase-dependent ground-state fermion parity. In this implementation, a major challenge is to quickly modulate the temperature of the proximitized QSH junction while preserving its fermion parity. While this condition precludes galvanic channels of heat transfer to the QSH system, others such as phononic[28], photonic[29,30], or radiative[24] channels could be used. In such set-ups, the timescale of the temperature modulation could be as low as 0.1 ns (see Supplementary Notes VII), much smaller than typical quasiparticle poisoning timescales, which are of the order of 1 µs[31–33]. Hence, implementing a parity conserving Josephson–Stirling cycle appears feasible. The work per cycle can be experimentally determined by measuring the current–phase relation during each isothermal process to compute the work integrals. Such current–phase measurements have, for example, been successfully performed in topological junctions with scanning superconducting quantum interference device microscopes[34,35] (see also Supplementary Notes VIII).

Conclusions. In this manuscript, we have explicitly discussed topological Josephson heat engines for the example of a short QSH-based Josephson junction. Since the concept is only based on the 4π-periodicity of the ground-state fermion parity, it is also applicable to long as well as nanowire-based topological Josephson junctions. Schemes to detect signatures of the 4π-periodic ground-state parity in topological Josephson junctions often require careful interpretation of the measurements[36,37]. It is therefore desirable to have several different, complementary approaches. As their properties reflect the 4π-periodic ground-state of topological Josephson junctions, topological Josephson heat engines could be used as such a complementary set-up to test the topological superconductivity as long as fermion parity can be conserved. However, even without conserving the ground-state fermion parity, topological Josephson junctions represent versatile machines with various operating modes.

Data availability

The data that support the findings of this study are available within the paper and its Supplementary Information. Additional data are available from the corresponding author upon request.

Received: 9 March 2020; Accepted: 1 October 2020;
Published online: 04 November 2020

References

1. Hasan, M. Z. & Kane, C. L. Colloquium: Topological insulators. *Rev. Mod. Phys.* **82**, 3045 (2010).
2. Qi, X.-L. & Zhang, S.-C. Topological insulators and superconductors. *Rev. Mod. Phys.* **83**, 1057 (2011).
3. Lutchyn, R. M., Sau, J. D. & Das Sarma, S. Majorana fermions and a topological phase transition in semiconductor-superconductor heterostructures. *Phys. Rev. Lett.* **105**, 077001 (2010).
4. Murthy, C. et al. Energy spectrum and current-phase relation of a nanowire Josephson junction close to the topological transition. *Phys. Rev. B* **101**, 224501 (2020).
5. Fu, L. & Kane, C. L. Superconducting proximity effect and Majorana fermions at the surface of a topological insulator. *Phys. Rev. Lett.* **100**, 096407 (2008).
6. Houzet, M., Meyer, J. S., Badiane, D. M. & Glazman, L. I. Dynamics of Majorana states in a topological Josephson junction. *Phys. Rev. Lett.* **111**, 046401 (2013).
7. Beenakker, C. W. J., Pikulin, D. I., Hyart, T., Schomerus, H. & Dahlhaus, J. P. Fermion-parity anomaly of the critical supercurrent in the quantum spin-hall effect. *Phys. Rev. Lett.* **110**, 017003 (2013).
8. Crépin, F. m. c. & Trauzettel, B. Parity measurement in topological Josephson junctions. *Phys. Rev. Lett.* **112**, 077002 (2014).
9. Sothmann, B., Giazotto, F. & Hankiewicz, E. M. High-efficiency thermal switch based on topological Josephson junctions. *New J. Phys.* **19**, 023056 (2017).
10. Tkachov, G., Burset, P., Trauzettel, B. & Hankiewicz, E. M. Quantum interference of edge supercurrents in a two-dimensional topological insulator. *Phys. Rev. B* **92**, 045408 (2015).
11. Murani, A. et al. Microwave signature of topological Andreev level crossings in a bismuth-based Josephson junction. *Phys. Rev. Lett.* **122**, 076802 (2019).
12. Rokhinson, L. P., Liu, X. & Furdyna, J. K. The fractional a.c. Josephson effect in a semiconductor-superconductor nanowire as a signature of Majorana particles. *Nat. Phys.* **8**, 795 (2012).
13. Wiedenmann, J. et al. 4π-periodic Josephson supercurrent in HgTe-based topological Josephson junctions. *Nat. Commun.* **7**, 10303 (2016).
14. Laroche, D. et al. Observation of the 4π-periodic Josephson effect in indium arsenide nanowires. *Nat. Commun.* **10**, 245 (2019).
15. Kayyalha, M. et al. Anomalous low-temperature enhancement of supercurrent in topological-insulator nanoribbon Josephson junctions: evidence for low-energy Andreev bound states. *Phys. Rev. Lett.* **122**, 047003 (2019).
16. Deacon, R. S. et al. Josephson radiation from gapless Andreev bound states in HgTe-based topological junctions. *Phys. Rev. X* **7**, 021011 (2017).
17. Giazotto, F., Heikkilä, T. T., Luukanen, A., Savin, A. M. & Pekola, J. P. Opportunities for mesoscopics in thermometry and refrigeration: physics and applications. *Rev. Mod. Phys.* **78**, 217 (2006).
18. Giazotto, F. & Martinez-Perez, M. J. The Josephson heat interferometer. *Nature* **492**, 401 (2012).
19. Fornieri, A., Blanc, C., Bosisio, R. & a. D'Ambrosio, S. Nanoscale phase engineering of thermal transport with a Josephson heat modulator. *Nat. Nanotechnol.* **11**, 258 (2016).
20. Fornieri, A. & Giazotto, F. Towards phase-coherent caloritronics in superconducting circuits. *Nat. Nanotechnol.* **12**, 944 (2017).
21. Virtanen, P., Vischi, F., Strambini, E., Carrega, M. & Giazotto, F. Quasiparticle entropy in superconductor/normal metal/superconductor proximity junctions in the diffusive limit. *Phys. Rev. B* **96**, 245311 (2017).
22. Vischi, F. et al. Thermodynamic cycles in Josephson junctions. *Sci. Rep.* **9**, 3238 (2019).
23. Vischi, F., Carrega, M., Braggio, A., Virtanen, P. & Giazotto, F. Thermodynamics of a phase-driven proximity Josephson junction. *Entropy* **21**, 1005 (2019).
24. Pendry, J. B. Radiative exchange of heat between nanostructures. *J. Phys. Condens. Matter* **11**, 6621 (1999).
25. Qiu, T. Q. & Tien, C. L. Heat transfer mechanisms during short-pulse laser heating of metals. *J. Heat. Transf.* **115**, 835 (1993).
26. Baffou, G. & Quidant, R. Thermo-plasmonics: using metallic nanostructures as nano-sources of heat. *Laser Photonics Rev.* **7**, 171 (2013).
27. Beenakker, C. W. J. in *Transport Phenomena in Mesoscopic Systems* (eds Fukuyama, H. & Ando T.) 235–253 (Springer, Berlin, 1992).
28. Li, N. et al. Colloquium: Phononics: manipulating heat flow with electronic analogs and beyond. *Rev. Mod. Phys.* **84**, 1045 (2012).
29. Bosisio, R., Solinas, P., Braggio, A. & Giazotto, F. Photonic heat conduction in Josephson-coupled Bardeen-Cooper-Schrieffer superconductors. *Phys. Rev. B* **93**, 144512 (2016).
30. Ronzani, A. et al. Tunable photonic heat transport in a quantum heat valve. *Nat. Phys.* **14**, 991 (2018).
31. Rainis, D. & Loss, D. Majorana qubit decoherence by quasiparticle poisoning. *Phys. Rev. B* **85**, 174533 (2012).
32. Virtanen, P. & Recher, P. Microwave spectroscopy of Josephson junctions in topological superconductors. *Phys. Rev. B* **88**, 144507 (2013).
33. Frombach, D. & Recher, P. Quasiparticle poisoning effects on the dynamics of topological Josephson junctions. *Phys. Rev. B* **101**, 115304 (2020).
34. Sochnikov, I. et al. Nonsinusoidal current-phase relationship in Josephson junctions from the 3D topological insulator HgTe. *Phys. Rev. Lett.* **114**, 066801 (2015).
35. Hart, S. et al. Current-phase relations of inas nanowire Josephson junctions: from interacting to multimode regimes. *Phys. Rev. B* **100**, 064523 (2019).

36. Dominguez, F. et al. Josephson junction dynamics in the presence of 2π- and 4π-periodic supercurrents. *Phys. Rev. B* **95**, 195430 (2017).
37. Chiu, C.-K. & Das Sarma, S. Fractional Josephson effect with and without Majorana zero modes. *Phys. Rev. B* **99**, 035312 (2019).

Acknowledgements

B.S. and E.M.H. acknowledge funding by the Deutsche Forschungsgemeinschaft (DFG, German Research Foundation) through SFB 1170, Project-ID 258499086, through Grant No. HA 5893/4-1 within SPP 1666 and through the Würzburg-Dresden Cluster of Excellence on Complexity and Topology in Quantum Matter – ct.qmat (EXC 2147, Project-ID 390858490) as well as by the ENB Graduate School on Topological Insulators. E.S., A.B., and F.G. acknowledge partial financial support from the EU's Horizon 2020 research and innovation program under Grant Agreement No. 800923 (SUPERTED), the CNR-CONICET cooperation program "Energy conversion in quantum nanoscale hybrid devices," the SNS-WIS jointlab QUANTRA funded by the Italian Ministry of Foreign Affairs and International Cooperation, and the Royal Society through the International Exchanges between the UK and Italy (Grant Nos. IES R3 170054 and IEC R2192166). This publication was supported by the Open Access Publication Fund of the University of Würzburg.

Author contributions

E.H. and F.G. conceived the idea of applying the concepts of heat engines to topological Josephson junctions. These concepts were then further developed and refined into the theoretical formulation presented in this work after intense discussions with B.S., A.B., and E. S. B.S. performed the calculations. All authors contributed to the writing of the manuscript.

Funding

Open Access funding enabled and organized by Projekt DEAL.

Competing interests

The authors declare no competing interests.

Additional information

Supplementary information is available for this paper at https://doi.org/10.1038/s42005-020-00463-6.

Correspondence and requests for materials should be addressed to B.S.

Reprints and permission information is available at http://www.nature.com/reprints

Publisher's note Springer Nature remains neutral with regard to jurisdictional claims in published maps and institutional affiliations.